

Analyzing Localizability of LEO/MEO Hybrid Networks: A Stochastic Geometry Approach

Ruibo Wang, *Member, IEEE*, Mustafa A. Kishk, *Member, IEEE*,
Howard H. Yang, *Member, IEEE*, and Mohamed-Slim Alouini, *Fellow, IEEE*

Abstract

With the increase in global positioning service demands and the requirement for more precise positioning, assisting existing medium and high orbit satellite-enabled positioning systems with low Earth orbit (LEO) satellites has garnered widespread attention. However, providing low computational complexity performance analysis for hybrid LEO/MEO massive satellite constellations remains a challenge. In this article, we introduce for the first time the application of stochastic geometry (SG) framework in satellite-enabled positioning performance analysis and provide an analytical expression for the K -availability probability and K -localizability probability under bidirectional beam alignment transmissions. The K -localizability probability, defined as the probability that at least K satellites can participate in the positioning process, serves as a prerequisite for positioning. Since the modeling of MEO satellite constellations within the SG framework has not yet been studied, we integrate the advantages of Cox point processes and binomial point processes, proposing a doubly stochastic binomial point process binomial point process for accurate modeling of MEO satellite constellations. Finally, we investigate the impact of constellation configurations and antenna patterns on the localizability performance of LEO, MEO, and hybrid MEO/LEO constellations. We also demonstrate the network performance gains brought to MEO positioning systems by incorporating assistance from LEO satellites.

Index Terms

Localizability, availability, stochastic geometry, doubly stochastic binomial point process, LEO satellite, MEO satellite.

Ruibo Wang and Mohamed-Slim Alouini are with King Abdullah University of Science and Technology (KAUST), CEMSE division, Thuwal 23955-6900, Saudi Arabia. Mustafa A. Kishk is with the Department of Electronic Engineering, Maynooth University, Maynooth, W23 F2H6, Ireland. Howard H. Yang is with the ZJU-UIUC Institute, Zhejiang University, Haining 314400, China. (e-mail: ruibo.wang@kaust.edu.sa; mustafa.kishk@mu.ie; haoyang@intl.zju.edu.cn; slim.alouini@kaust.edu.sa). Corresponding author: Howard H. Yang.

I. INTRODUCTION

Over the years, satellite-enabled positioning services have been primarily enabled by medium Earth orbit (MEO) satellites and a small number of geosynchronous Earth orbit (GEO) satellites. Indeed, positioning technologies based on MEO has been mature, achieving extensive coverage as well as global positioning with a small number of satellites [1]. However, the already deployed satellite constellations may face challenges in expanding their capabilities when addressing the demands of future networks for low latency and high-precision positioning, as well as the increasing requirements for additional positioning services [2]. Involving the deployment of mega LEO satellite constellations in auxiliary positioning is a potential solution [3]. Compared to MEO satellites, LEO satellites orbit at a closer distance to the Earth, resulting in lower positioning latency [4], [5]. Besides, since the carrier frequencies used by LEO satellites are different from those for MEO satellite-enabled positioning systems [6], the two systems do not interfere with each other while positioning errors can be reduced with an increased number of satellites in use [7]. Therefore, leveraging LEO satellites in existing MEO-based systems to improve positioning performance is a topic worthy of research.

Nonetheless, assessing the performance of such an integration poses new challenges. More precisely, the performance of traditional MEO satellite-enabled positioning systems is chiefly evaluated based on simulations. Specifically, researchers use simulation software to generate the positions of satellites at a particular moment [8]. Performance testing of proposed algorithms and analytical results is then conducted based on these simulated satellite positions [9], [10]. To ensure the reliability of the results, the above procedures need to be executed in numerous rounds to validate the performance gain under various satellite topologies [11]. Compared to MEO constellations, analyzing the performance of positioning in a hybrid LEO/MEO satellite system is more difficult. Currently, the number of satellites in medium to high Earth orbit global positioning systems is only a few dozen, making simulation-based satellite position modeling reasonable [1]. However, the proliferation of mega-constellations of LEO satellites, numbering in the hundreds or even thousands, significantly increases computational complexity [12]. An effective solution is to establish an analytical framework to directly map the satellite system's parameters to positioning-related metrics, such as satellite diversity and accuracy of positioning. Among various mathematical tools, stochastic geometry (SG) is particularly well-suited for establishing the aforementioned analytical framework, as it is also one of the few tools capable

of interference analysis in large-scale random network topology [13].

A. Related Works

In this subsection, we briefly review existing research on SG-based satellite modeling and SG-based positioning for terrestrial networks, emphasizing the foundation upon which this article is built, along with their limitations.

In recent years, there have been studies employing SG for modeling and analyzing LEO satellite networks under the SG framework [14], [15]. Among the SG-based models, the spherical binomial point process (BPP) is one of the most widely applied models for LEO satellite constellations. The BPP requires only the altitude of the constellation and the number of satellites, to model the LEO satellite constellation [16]. However, compared to real-world constellations, the accuracy of BPP modeling diminishes with a decrease in the number of satellites [17]. Although the BPP model has been shown to align with real-world constellations in terms of performance evaluation for massive LEO constellations containing thousands of satellites [18], it is not a suitable modeling approach for MEO constellations that consist of only dozens of satellites.

Furthermore, the Cox point process (CPP) model proposed by the authors in [19], [20] offers inspiration for modeling MEO satellite constellations. Although the CPP model is still applied to modeling mega LEO constellations, it takes into account the reality of satellites operating on orbits, thus making it more accurate than BPP. CPP assumes that both the number of orbits and the number of satellites per orbit follow a Poisson distribution [19]. Authors in [21], by simplifying the CPP model to a constellation with a single orbit and applying it to GEO satellite modeling, have demonstrated to some extent that orbit-based models are more reasonable and accurate for modeling smaller-scale constellations like MEO. While the performance differences between the Poisson distribution and the binomial distribution become negligible when the number of satellites is large, a MEO constellation typically consists of only several orbits with each orbit hosting several satellites. In such cases, modeling the number of orbits and the number of satellites per orbit as random Poisson distributions deviates from the deterministic reality of satellite constellations, leading to discrepancies between the model and the actual deterministic constellation model. Hence, it is necessary to propose a more accurate SG-based model for MEO constellations with a limited number of satellites.

So far, researchers have established analytical frameworks for positioning in planar networks under the SG framework. Among them, almost all of the studies analyzed the localizability probability, as it is one of the most fundamental and important metrics for localization [22], [23]. The K -localizability probability is defined as the probability that a target can detect at least K signals [24]. It is worth noting that the definition of "localizability" in satellite-enabled positioning systems differs significantly from that of terrestrial-based positioning systems. Since single-satellite localization will be used in practice, satisfying K -localizability ($K > 1$) does not necessarily mean that the positioning system requires the detection of at least K satellites to function properly. Considering the mentioned fact that the more satellites are involved in positioning, the better the performance and the higher the accuracy, we have continued to use the concept of localizability in satellite-enabled positioning. In this context, K -localizability is used to measure the quality of localization performance rather than the feasibility of the positioning system's operation.

In addition, the analysis of satellite networks also differs significantly from that of terrestrial networks. Satellites are deployed on a spherical surface, making the analytical expression of distance distribution more complicated [25] than the planar network. Satellites are equipped with antennas emitting directional signals, making interference analysis challenging [26]. Furthermore, only satellites not blocked by the Earth can participate in positing, making satellite availability a prerequisite for localizability [27].

B. Contribution

To our knowledge, this is the first article that applies the SG framework in the localizability analysis of satellite networks. The contributions of this article are as follows.

- This is the first study of MEO satellite constellations modeling and analysis under the SG framework. We propose a doubly stochastic binomial point process (DSBPP) for modeling MEO satellites. Specifically, an underlying BPP is generated and mapped to the positions of orbits, with satellites on each orbit following a BPP distribution based on the underlying BPP. Compared to CPP, DSBPP provides a more accurate modeling of MEO constellations without decreasing the tractability.
- For interference mitigation considerations, we adopt a bi-directional aligned beam model and provide a general representation for modeling antenna gains. Because existing literature

on the spherical SG framework primarily discusses unidirectional beam alignment, our analytical framework can offer guidance for subsequent bidirectional alignment.

- Based on this model, we derive analytical expressions for availability and estimate the localizability of satellite-enabled positioning systems under the precondition of satellite availability. The above analytical results are of low complexity and verified to be accurate.
- Finally, the impacts of constellation configurations such as constellation altitude, and physical-level parameters such as antenna patterns on network performance are studied. In addition, we demonstrate that a hybrid MEO/LEO constellation offers better localizability performance compared to an MEO constellation without the assistance of LEO satellites.

II. SYSTEM MODEL

This section provides the LEO and MEO satellite spatial distribution models, antenna gain pattern models, and the satellite-terrestrial channel model. A schematic diagram for the system model is shown in Fig. 1.

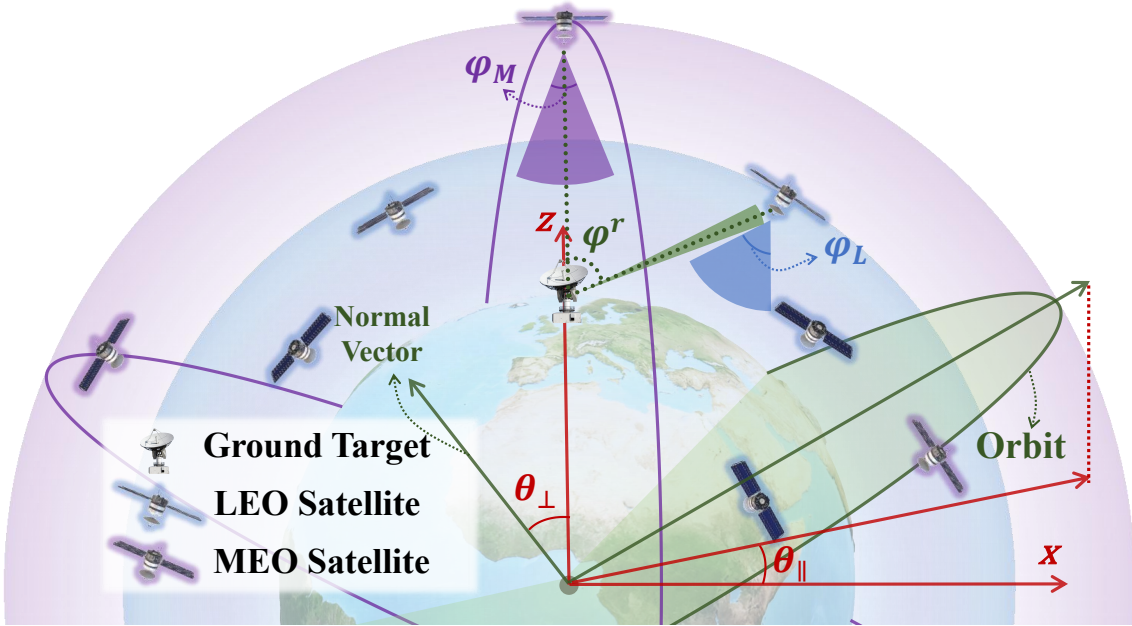


Fig. 1: Schematic diagram for the system model.

A. Spatial Distribution

We consider a hybrid positioning system composed of an LEO satellite constellation and an MEO satellite constellation. The LEO satellite constellation consists of N_L satellites distributed

on a sphere around Earth, forming a homogeneous spherical BPP. The distance between the LEO satellite and Earth's center is denoted as R_L . According to Slivnyak's theorem, homogeneous BPP is rotation invariant [28]. In other words, the rotation of the coordinate system does not affect the LEO satellite distribution. Therefore, we take the Earth's center as the origin. Without loss of generality, the coordinates of a typical ground target in the spherical coordinate system as $(R_\oplus, 0, 0)$, where $R_\oplus = 6371$ km is the radius of the Earth. The azimuth angle and polar angle of the ground target are both 0.

The MEO satellite constellation comprises N_o orbits, with N_M satellites on each orbit. The distance between the MEO satellite and Earth's center is denoted as R_M . The position of an orbit can be uniquely determined by its azimuth angle θ_\parallel and inclination angle θ_\perp relative to the ground target. Note that due to our focus on the position of the orbit relative to the ground target, these two angles differ from their definitions in astrodynamics. As shown in Fig. 1, the inclination angle θ_\perp of an orbit is the angle between the positive z -axis direction and the normal vector of the orbital plane. The positive z -axis direction refers to the direction from the origin to the target. The probability density function (PDF) of θ_\perp is given as

$$f_{\theta_\perp}(\theta) = \frac{\sin \theta}{2}, \quad 0 \leq \theta < \pi. \quad (1)$$

Then, we connect the origin to the point on the orbit closest to the target and obtain a segment. We project this segment onto the xy -plane, and the angle formed by the projected segment and the positive x -axis is referred to as the azimuth angle θ_\parallel . Furthermore, θ_\parallel is assumed to follow a uniform distribution, i.e., $\theta_\parallel \sim \mathcal{U}[0, 2\pi)$. By making a simple extension of the conclusions from [19], it can be proved that θ_\perp and θ_\parallel are also rotation invariant. As such, for an arbitrary ground reference position, the PDFs of θ_\perp and θ_\parallel relative to that position remain consistent.

As for the spatial distribution of MEO satellites, the N_M satellites on each orbit are uniformly distributed along the orbit, forming a one-dimensional BPP. According to [19], the spatial distribution of orbits is mapped from a two-dimensional BPP. Therefore, the positions of MEO satellites in a single orbit are mapped from a one-dimensional BPP generated based on a two-dimensional BPP as the underlying point process. As a result, the positions of MEO satellites in the constellation follow a DSBPP.

B. Antenna Pattern

Given that satellites and the target are equipped with directional antennas. Satellites are equipped with wide spherical beams. The beam is directed toward the sub-satellite point, which

is the intersection point between the Earth's surface and the line connecting the Earth's center to the satellite. Given the challenge of effectively covering targets situated at considerable distances from the sub-satellite point, we have established maximum central communication angles for LEO and MEO satellites, denoted by φ_L and φ_M respectively. As shown in Fig. 1, when the angle formed between the line connecting the satellite to the user and the line connecting the satellite to the Earth's center exceeds $\varphi_L/2$ or $\varphi_M/2$, the satellite cannot be effectively used for precise positioning. In addition, the antenna gains of LEO satellites and MEO satellites are denoted as G_L^t and G_M^t , respectively.

The ground target aligns the beams toward the associated satellites, including MEO and LEO satellites involved in positioning. The satellite association strategy, also known as the beam alignment strategy, will be demonstrated in Sec. III-B Proposition 2. For each beam, or for each alignment, the signal from the aligned satellite is the target signal and signals from all other satellites are considered interference. It is worth emphasizing that a satellite involved in positioning belongs to the target satellite for a specific beam or alignment, while at other times, it acts as an interfering satellite.

Then, we assume that the antenna patterns of the target are circularly symmetric, with the gain of a single antenna denoted as $G^r(\varphi^r)$. The aligned satellite receives the maximum beam gain G_Q^m , i.e., $G^r(0) = G_Q^m$. φ^r is the dome angle between the associated satellite and the interfering satellite. Fig. 1 illustrates an example of φ^r . When the ground target aligns with a LEO satellite, φ^r is formed between the line connecting the target to the associated LEO satellite and the line connecting the target to the interfering MEO satellite. The receiving beam gain $G^r(\varphi^r)$ decreases monotonically as φ^r increases and the interference can be eliminated by directing the receiving beams toward the expected signals. For interference mitigation purposes, the directional receiving beam of the target shall be narrower than the satellite's wide beam.

C. Channel Model

We consider that the satellite-terrestrial link follows the free space fading model, experiencing large-scale fading and small-scale fading. This channel model framework is considered to be applicable to both LEO satellites and MEO satellites for downlinks to the ground [19]. In this case, the target's received power is [16]

$$\rho_Q^r = \begin{cases} \rho_Q^t G_Q^t G^r(\varphi^r) \zeta \left(\frac{\lambda_Q}{4\pi} \right)^2 l^{-2} W, & l \leq d_Q^{\max}, \\ 0, & \text{otherwise,} \end{cases} \quad (2)$$

where ρ_Q^t , ζ , λ_Q , and l denote the transmit power, the system loss caused by the atmosphere, the wavelength, and the distance between satellite and target, respectively. d_Q^{\max} is the maximum distance at which the target can detect the signals from satellites. Details of d_Q^{\max} will be discussed in the next section. If (2) represents the LEO satellite-target link, Q is replaced by L ; otherwise, for the MEO satellite-target link, Q is replaced by M .

Finally, we assume that the small-scale fading W follows shadowed Rician (SR) fading, which is considered to be the most accurate small-scale fading model for space-terrestrial link [29]. The cumulative distribution function (CDF) of small-scale fading is given as follows:

$$F_W(w) = \left(\frac{2b_0m}{2b_0m + \Omega} \right)^m \sum_{z=0}^{\infty} \frac{(m)_z}{z! \Gamma(z+1)} \left(\frac{\Omega}{2b_0m + \Omega} \right)^z \Gamma_l \left(z+1, \frac{w}{2b_0} \right), \quad (3)$$

where $(m)_z$ is the Pochhammer symbol, m , b_0 , and Ω respectively denote the Nakagami parameter, average power of the line-of-sight (LoS) component, and the average power of the multi-path component. $\Gamma(\cdot)$ and $\Gamma_l(\cdot, \cdot)$ denote the gamma function and lower incomplete gamma function, respectively. Furthermore, the PDF of small-scale fading can be expressed as:

$$f_W(w) = \left(\frac{2b_0m}{2b_0m + \Omega} \right)^m \frac{\exp\left(-\frac{w^2}{2b_0}\right)}{2b_0} {}_1F_1 \left(m, 1, \frac{\Omega m}{2b_0(2b_0m + \Omega)} \right), \quad (4)$$

where ${}_1F_1(\cdot, \cdot, \cdot)$ is the Confluent Hypergeometric function.

III. LOCALIZABILITY ANALYSIS

This section presents the definition and analytical expression of availability probability, contact angle distribution, interference power, and localizability probability. The theoretical framework is applicable not only to the analysis of hybrid LEO/MEO satellite constellations but also to pure LEO constellations or MEO constellations.

A. Availability Probability

This section derives the availability probability for hybrid LEO/MEO satellite networks. For ease of derivation, we first define the central angle.

Definition 1. *The central angle between A and B refers to the angle created by the line connecting A to the Earth's center and the line connecting B to the Earth's center.*

To detect the signal from the satellite, the target needs to be within the satellite's main lobe. Furthermore, the target and the satellite need to establish a LoS link, i.e., the link cannot be

blocked by the Earth. As such, we can derive the upper limit of central angle θ_Q^{\max} between the satellite and target, given in the following lemma.

Lemma 1. *The maximum central angle at which the target can detect the signals from the satellite is*

$$\theta_Q^{\max} = \begin{cases} \arccos\left(\frac{R_{\oplus}}{R_Q}\right), & \text{when } \varphi_Q \geq 2 \arcsin\left(\frac{R_{\oplus}}{R_Q}\right), \\ \arcsin\left(\frac{R_Q \sin(\varphi_Q/2)}{R_{\oplus}}\right) - \frac{\varphi_Q}{2}, & \text{otherwise.} \end{cases} \quad (5)$$

where Q is substituted with L for LEO satellites and M for MEO satellites.

Proof: See Appendix A. ■

Then, we can establish the relationship between the maximum detectable central angle θ_Q^{\max} and the maximum detectable distance d_Q^{\max} , as

$$d_Q^{\max} = \sqrt{R_Q^2 + R_{\oplus}^2 - 2R_Q R_{\oplus} \cos \theta_Q^{\max}}, \quad Q = \{L, M\}. \quad (6)$$

Consequently, we define the following K –availability probability.

Definition 2 (K –Availability Probability). *K –availability probability refers to the probability of having at least K satellites available for the ground target. When an LEO or MEO satellite is available, it has a distance less than d_L^{\max} or d_M^{\max} from the target.*

As shown in Definition 2, d_Q^{\max} can make the definition more intuitively and clearly expressed. However, as will be clear from the upcoming analysis, using central angles θ_Q^{\max} instead of Euclidean distance d_Q^{\max} is more concise in derivations.

Lemma 2. *K –availability probability for LEO satellites can be calculated as,*

$$P_L^A(K) = 1 - \sum_{k=0}^{K-1} \binom{N_L}{k} \left(\frac{1 - \cos \theta_L^{\max}}{2}\right)^k \left(\frac{1 + \cos \theta_L^{\max}}{2}\right)^{N_L-k}. \quad (7)$$

Proof: See Appendix B. ■

After computing the K –availability probability for LEO satellites, the next step is to derive the same quantity for MEO satellites. First, we present the maximum central angle of a given orbit in Lemma 3.

Lemma 3. *Given that two satellites are located in an orbit with inclination angle θ_\perp , and these two satellites are at a distance less than d_M^{\max} from the target, the maximum central angle between them is*

$$\theta_{c,M}^{\max}(\theta_\perp, d_M^{\max}) = \begin{cases} 2 \arccos\left(\frac{R_\oplus^2 + R_M^2 - (d_M^{\max})^2}{2R_\oplus R_M \sin \theta_\perp}\right), \\ \text{when } \left|\theta_\perp - \frac{\pi}{2}\right| \leq \arccos\left(\frac{R_\oplus^2 + R_M^2 - (d_M^{\max})^2}{2R_\oplus R_M}\right), \\ 0, \text{ otherwise.} \end{cases} \quad (8)$$

Proof: See Appendix C. ■

Lemma 1 can be regarded as the unconditional upper limit of the central angle, while Lemma 3 represents the upper limit of the central angle given a specific orbit. Based on Lemma 3, the K -availability of MEO satellites is derived as follows.

Lemma 4. *K -availability probability for MEO satellites is*

$$P_M^A(K) = 1 - \sum_{k=0}^{K-1} \binom{N_M N_O}{k} (p_{M,1}^A)^k (1 - p_{M,1}^A)^{N_M N_O - k}, \quad (9)$$

where $p_{M,1}^A$ is the probability that a given MEO satellite is available for the target, given by

$$p_{M,1}^A = \int_{\frac{\pi}{2} - \arccos\left(\frac{R_\oplus^2 + R_M^2 - (d_M^{\max})^2}{2R_\oplus R_M}\right)}^{\frac{\pi}{2} + \arccos\left(\frac{R_\oplus^2 + R_M^2 - (d_M^{\max})^2}{2R_\oplus R_M}\right)} \frac{\theta_{c,M}^{\max}(\theta, d_M^{\max}) \sin \theta}{4\pi} d\theta. \quad (10)$$

Proof: See Appendix D. ■

Finally, the following theorem provides the analytical expression of K -availability probability based on the Lemma 2 and Lemma 4.

Theorem 1. *The K -availability probability for hybrid LEO/MEO satellite networks is given by*

$$P_{\text{all}}^A(K) = \sum_{k=0}^{\min\{K-1, N_M^{\max}-1\}} P_L^A(K-k) p_M^A(k) + \sum_{k=K}^{\max\{K, N_M^{\max}\}} p_M^A(k), \quad (11)$$

where N_M^{\max} is predefined upper limit of available MEO satellites, and $P_L^A(K)$ is given in Lemma 2. $p_M^A(k)$ is the probability that exactly k MEO satellites are available for the target,

$$p_M^A(k) = \binom{N_M N_O}{k} (p_{M,1}^A)^k (1 - p_{M,1}^A)^{N_M N_O - k}. \quad (12)$$

Proof: See Appendix E. ■

$N_M^{\max} \ll N_M N_O$ is set to reduce computational complexity. The satellite deployment density in MEO constellations is usually lower than that in LEO constellations. Therefore, setting an

upper limit for MEO satellites is more effective in reducing computational complexity compared to LEO satellites.

Proposition 1. *A criterion regarding the recommended value for N_M^{\max} is given as follows:*

$$N_M^{\max} = \arg \min_K \left\{ 1 - \sum_{k=0}^K p_M^A(k) \leq \varepsilon \right\}, \quad (13)$$

where ε is a positive real value close to 0.

We set $\varepsilon = 0.01$ in this article; namely, the probability of having more than N_M^{\max} available MEO satellites is less than 1%.

B. Contact Angle Distribution

This subsection elaborates on the association strategy for the ground target and the contact angle distributions for LEO and MEO satellites. In satellite-enabled positioning systems, accuracy can be enhanced by utilizing consecutive positioning results from the same satellite, e.g., the Kalman filtering technique employed in the GPS system [30]. To minimize the cost of beam scanning, a beam is generally associated with a specific satellite during a period rather than switching satellites frequently. In the following proposition, we provide the association strategy adopted by this article.

Proposition 2. *Considering the maturity of the positioning technology of MEO satellites, the beams of the ground target are prioritized to associate with available MEO satellites, while the remaining beams are sequentially associated with the nearest LEO satellites.*

This association strategy is designed from the perspective of an LEO-assisted MEO satellite-enabled positioning system. Notice that the localizability analysis based on the associated strategy depends on the relative distance between the associated satellite and the target. Therefore, we propose the concept of the contact angle to measure this relative distance.

Definition 3 (Contact Angle). *The central angle between the target and its k^{th} nearest LEO satellite is referred to as the k -LEO contact angle. The central angle between an MEO satellite and the target is referred to as the MEO contact angle.*

Then, the PDFs of the contact angle distributions are derived in the following lemmas.

Lemma 5. *The PDF of the K -LEO contact angle distribution is given as,*

$$f_{\theta_L}^{(K)}(\theta) = 1 - \frac{\sin \theta}{2^{N_L}} \sum_{n=0}^{K-1} \binom{N_L}{n} (1 - \cos \theta)^n \times (1 + \cos \theta)^{N_L-n} \left(\frac{n}{1 - \cos \theta} - \frac{N_L - n}{1 + \cos \theta} \right), \quad (14)$$

where $0 \leq \theta \leq \theta_L^{\max}$.

Proof: See Appendix F. ■

Lemma 6. *The PDF of the MEO contact angle distribution is given as,*

$$f_{\theta_M}(\theta) = \frac{\sin \theta}{\pi} \int_{\frac{\pi}{2}-\theta}^{\frac{\pi}{2}} \frac{1}{\sqrt{\sin^2 \theta_{\perp} - \cos^2 \theta}} d\theta_{\perp}, \quad (15)$$

where $0 \leq \theta \leq \theta_M^{\max}$.

Proof: See Appendix G. ■

Toward this end, we have finished the analysis from the topological perspective. In the next subsection, we delve into the channel aspect and introduce K -localizability probability for further analysis.

C. Localizability Probability

This subsection provides the definition of K -localizability probability and derives the analytical expression of interference power and K -localizability probability.

Definition 4 (K -Localizability Probability). *K -localizability probability is defined as the probability that the K associated satellites' instantaneous received Signal-to-interference-plus-noise ratios (SINRs) at the target are all greater than the threshold γ_L for LEO satellites or γ_M for MEO satellites.*

The mathematical definition of K -localizability probability can be expressed by the following formula:

$$P_{\text{all}}^L(K) = \prod_{k=1}^K \mathbb{P} \left[\text{SINR}_k = \frac{\rho_{Q,k}^r}{I_k + \sigma_Q^2} > \gamma_Q \right], \quad (16)$$

where SINR_k is the instantaneous received SINR of the k^{th} associated satellite. Q is replaced with M when the k^{th} associated satellite is an MEO satellite; otherwise, Q is replaced with L . $\rho_{Q,k}^r$ is the received power of the k^{th} associated satellite. Its randomness is caused by the contact

$$f_I(I) = \int_0^{\theta_d^{\max}} f_W \left(\frac{I (R_L^2 + R_{\oplus}^2 - 2R_L R_{\oplus} \cos \theta_L)}{\rho_L^t G_L^t \zeta \left(\frac{\lambda_L}{4\pi} \right)^2 G^r \left(\cot^{-1} \left(\cot \theta_I - \frac{R_{\oplus}}{R_L} \sqrt{1 + \cot^2 \theta_I} \right) \right)} \right) \times \frac{(R_L^2 + R_{\oplus}^2 - 2R_L R_{\oplus} \cos \theta_L)}{\rho_L^t G_L^t \zeta \left(\frac{\lambda_L}{4\pi} \right)^2 G^r \left(\cot^{-1} \left(\cot \theta_I - \frac{R_{\oplus}}{R_L} \sqrt{1 + \cot^2 \theta_I} \right) \right)} \frac{\sin \theta_I}{1 - \cos \theta_d^{\max}} d\theta_I. \quad (19)$$

angle distribution and SR fading. σ_Q^2 is a constant representing the noise power. Moreover, I_k is the total interference power received by the target when the beam is aligned with the k^{th} associated satellite. Apart from the aligned satellite, the received power from other satellites is regarded as interference. Notably, since the LEO and MEO satellite-enabled positioning systems use different carrier frequencies, there is no mutual co-channel interference [6]. The following lemma estimates the approximate distribution of interference power.

Lemma 7. *Given that the central angle between the associated satellite and the target is θ , the interference power of the LEO satellite constellation can be expressed as a mixed random variable $I(\theta)$. The probability that $I(\theta)$ can be approximated as 0 is*

$$\mathbb{P}[I(\theta) \approx 0] = \left(\frac{1 + \cos \theta_d^{\max}}{2} \right)^{N_L}, \quad (17)$$

where θ_d^{\max} can be expressed as,

$$\theta_d^{\max} = \cot^{-1} \left(\frac{R_L^2}{R_L^2 - R_{\oplus}^2} \left(\cot \varphi_{\max} + \sqrt{(R_{\oplus}/R_L)^2 (1 + \cot^2 \varphi_{\max} - (R_{\oplus}/R_L)^2)} \right) \right). \quad (18)$$

φ_{\max} in (18) is defined as the effective receiving beam range.

When $I(\theta) \neq 0$, the PDF of $I(\theta)$ is shown in (19) at the top of the next page.

Proof: See Appendix H. ■

It is noteworthy that the interference power cannot actually be zero. However, under the premise of directional reception, when the interference power is negligible compared to noise, we can approximate it as zero. Due to the much lower density of MEO satellite deployment compared to LEO, as indicated in Appendix H, the probability of interference power being approximated as 0 is high. Furthermore, it is easier to avoid co-channel interference through frequency coordination. Therefore, we neglect the impact of interference from MEO constellations

on the localizability. Based on the contact angle distributions and interference power distribution, the analytical expressions of K -localizability probability can be given in the following lemmas and theorem.

Lemma 8. K -localizability probability for LEO satellites can be calculated as,

$$P_L^C(K) = \prod_{k=1}^K \int_0^{\theta_L^{\max}} f_{\theta_L}^{(k)}(\theta) \int_0^\infty f_I(I) \left(1 - F_W \left(\left(\frac{4\pi}{\lambda_L} \right)^2 \times \frac{\gamma_L (I + \sigma_L^2) (R_L^2 + R_\oplus^2 - 2R_L R_\oplus \cos \theta_L)}{\rho_L^t G_L^t G_L^m \zeta} \right) \right) dI d\theta_L. \quad (20)$$

Proof: See Appendix I. ■

The analytical expression in the above lemma can be regarded as an estimation of K -localizability for the hybrid LEO/MEO satellite network when no MEO satellites are available. On the contrary, the following lemma corresponds to the K -localizability when localization can be achieved without the assistance of LEO satellites.

Lemma 9. K -localizability probability for MEO satellites can be calculated as,

$$P_M^C(K) = 1 - \sum_{k=0}^{K-1} \binom{N_M N_O}{k} (p_{M,1}^C)^k (1 - p_{M,1}^C)^{N_M N_O - k}, \quad (21)$$

where $p_{M,1}^C$ is the probability that the target is localizable for a given MEO satellite,

$$p_{M,1}^C = \int_0^{\theta_M^{\max}} f_{\theta_M}(\theta) \left(1 - F_W \left(\gamma_M \left(\frac{4\pi}{\lambda_M} \right)^2 \times \frac{\sigma_M^2 (R_M^2 + R_\oplus^2 - 2R_M R_\oplus \cos \theta_M)}{\rho_M^t G_M^t G_M^m \zeta} \right) \right) d\theta_M. \quad (22)$$

Proof: The proof of Lemma 9 is similar to that of Lemma 4 and Lemma 8, therefore omitted here. ■

Next, we provide the results of the localizability probability for hybrid satellite networks.

Theorem 2. K -localizability probability for hybrid LEO/MEO satellite networks can be calculated as,

$$P_{\text{all}}^C(K) = \sum_{k=0}^{\min\{K-1, N_M^{\max}-1\}} P_L^C(K-k) p_M^C(k) + \sum_{k=K}^{\max\{K, N_M^{\max}\}} p_M^C(k), \quad (23)$$

where N_M^{\max} is defined in Theorem 1 and Proposition 1. $p_M^C(k)$ is the probability that the target is localizable for exactly k MEO satellites,

$$p_M^C(k) = \binom{N_M N_O}{k} (p_{M,1}^C)^k (1 - p_{M,1}^C)^{N_M N_O - k}. \quad (24)$$

Proof: The proof of Theorem 2 is similar to that of Theorem 1, therefore omitted here. ■

The above results demonstrate that the expressions for the localizability probability, whether in LEO, MEO, or hybrid constellations, all contain only double integrals, indicating an acceptable level of computational complexity. Finally, as shown in the Theorem 1 and the Theorem 2, the K -availability probability and K -localizability probability of the hybrid LEO/MEO satellite network involve single integral and double integrals, respectively. Considering the complex distance analysis due to spherical topology and the complex interference analysis caused by beam pointing, the analytical results in this paper are computationally inexpensive, with a complexity equivalent to or lower than that of most current research in the domain of spherical SG.

TABLE I: System parameters [2], [16], [31].

Notation	Physical meaning	Default value
h_L, h_M	Altitude of the satellite relative to the Earth's surface	1000 km, 20000 km
N_L	Number of LEO satellites	2000
N_o	Number of orbits (for MEO satellites)	2
N_M	Number of satellites on an orbit (for MEO satellites)	6
φ_L, φ_M	Maximum central communication angle	$\pi/4, \pi/6$
λ_L, λ_M	Wavelength	0.0150 m, 0.190 m
ρ_L^t, ρ_M^t	Transmission power	15 dBW, 18 dBW
G_L^t, G_M^t	Transmitting antenna gain	33.8 dBi, 24.1 dBi
G_L^m, G_M^m	Maximum receiving antenna gain	31.8 dBi, 5 dBi
ζ	System loss	−6 dB
σ_L^2, σ_M^2	Noise power	−90.2 dBm, −103.9 dBm
γ_L, γ_M	Coverage threshold	10 dBi, −16 dBi
φ_{3dB}	Half-power beamwidth	8 degree
(Ω, b_0, m)	Parameters of SR fading	(1.29, 0.158, 19.4)

IV. NUMERICAL RESULTS

This section presents the numerical results of K -availability probability and K -localizability probability. The overlap between the results obtained from Monte Carlo simulations (lines) and the derived analytical results (marks) in the figures validates the accuracy of the analytical results in this article.

A. Parameter Setting

To visually demonstrate the impact of altitude on performance, in this section, we define $h_Q = R_Q - R_\oplus$ as the altitude of the satellite relative to the Earth's surface, where $Q = \{L, M\}$. In addition, we apply the Gaussian antenna pattern [32] for the target's beam, and the receiving gain can be expressed as

$$G^r(\varphi^r) = G_Q^m 2^{-(\varphi^r)^2/\varphi_{3\text{dB}}^2}, \quad (25)$$

where $\varphi_{3\text{dB}}$ denotes half-power beamwidth of the receiving beam. Unless otherwise stated, other parameters will be set to their default values as Table I. The following are some explanations of the setting in Table I. The configuration of the number of orbits N_o and the number of satellites on an orbit N_M applies only to MEO satellite constellations.

Considering that satellite systems typically focus more on frequency rather than wavelength, we declare that in the numerical results corresponding to the cases in this section, the LEO satellites are concerned with the 20 GHz frequency band, i.e., the Ka-band, while the MEO satellites operate at 1.579 GHz, i.e., the L-band. In this case, the corresponding Wavelengths in the above analytical framework are set as $\lambda_L = 0.0150$ m and $\lambda_M = 0.190$ m.

B. Availability Probability

This subsection provides the numerical results of K -availability probabilities for LEO, MEO, and hybrid satellite networks. As shown in Fig. 2, the altitude of the satellite constellation h_s has a significant impact on the K -availability probability for LEO satellites. When $h_s = 2000$ km, a constellation of more than 3000 LEO satellites can provide at least 6 available satellites. However, even with 4000 satellites, a mega constellation with altitude $h_s = 1000$ km still cannot completely ensure the basic positioning requirements (typically, it requires 3 or 4 available satellites for positioning, depending on the specific positioning technology).

As revealed by Fig. 3, the number of MEO satellites required to achieve the same availability probability is much lower than that of LEO satellites. At an altitude of 20000 km, 24 satellites (the minimum operational number for GPS) can guarantee 4-availability, while 31 satellites (the typical operational number for GPS) can generally meet 6-availability. With the same number of satellites, deploying them at 20000 km altitude results in a 5% to 15% increase in availability probability compared to 10000 km altitude.

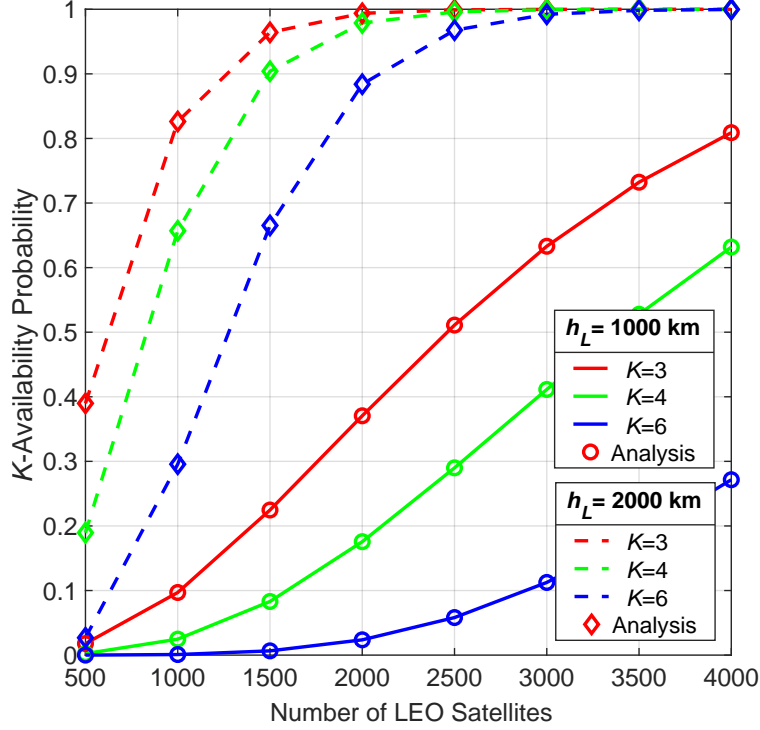


Fig. 2: K -availability probability for LEO satellites.

Fig. 4 examines the impact of altitude on a hybrid LEO/MEO satellite constellation. Compared to a constellation with 12 MEO satellites at an altitude of $h_M = 20000$ km, the hybrid constellation with extra 2000 LEO satellites at an altitude of $h_L = 1500$ km shows a 10%, 28%, 64% increase in 3, 4, 6-availability probability, respectively. We also find that when the availability probability is low, increasing the altitude of the LEO satellite constellation can bring a significant improvement to satellite availability.

Fig. 5 displays the influence of the number of satellites on 6-availability probability using a heatmap. The values of the points on the heatmap are calculated based on Theorem 1 (whose accuracy has been validated). The color boundaries in Fig. 5 are almost parallel to the main diagonal of the heatmap, indicating that the MEO and LEO satellites have a complementary relationship in terms of achieving availability. Specifically, for each MEO satellite decreased, it is necessary to add around 150 LEO satellites to maintain the 6-availability probability for the hybrid constellation.

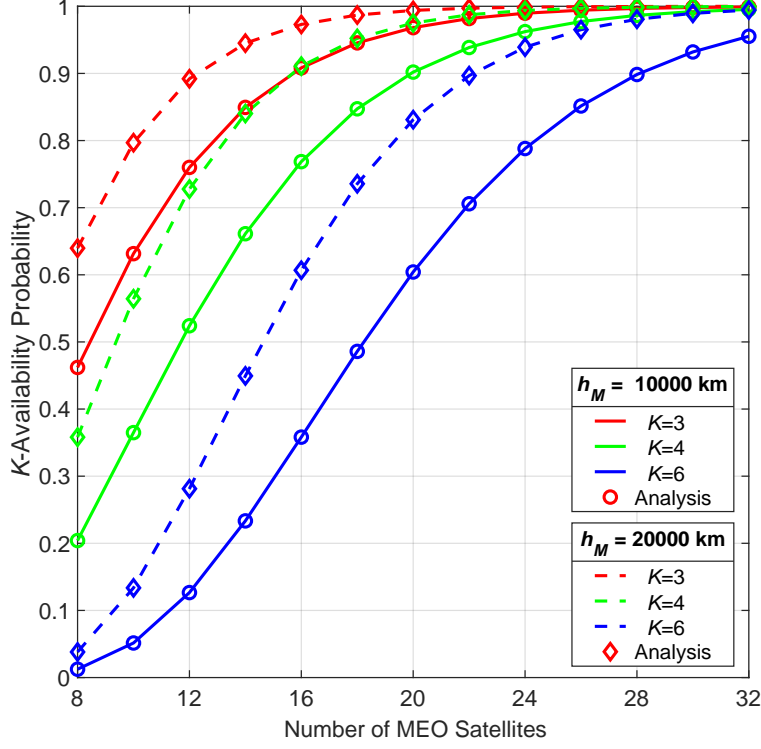


Fig. 3: K -availability probability for MEO satellites.

C. Localizability Probability

This subsection provides the numerical results of K -localizability probabilities for LEO, MEO, and hybrid satellite networks. Fig. 6 reveals that with an increase in the number of LEO satellites, the K -localizability probability exhibits two different trends depending on the altitude of satellite deployment. Specifically, when $h_L = 1000$ km, availability remains the dominant factor in determining the K -localizability probability. Therefore, as the number of satellites increases, the K -localizability probability monotonically increases. When $h_L = 2000$ km, the K -localizability probability initially increases due to the rise in K -availability probability. However, once availability nears 100%, interference becomes the decisive factor affecting the K -localizability probability, leading to a decline in the K -localizability probability as the number of satellites continues to increase. When the number of satellites is less than 4000, deploying them at a relative altitude of $h_L = 2000$ km has an advantage in terms of localizability compared to $h_L = 1000$ km.

Comparing the numerical results in Fig. 6 and Fig. 7, we can conclude that a constellation with 30 MEO satellites has an advantage over a constellation with 3000 LEO satellites in terms of

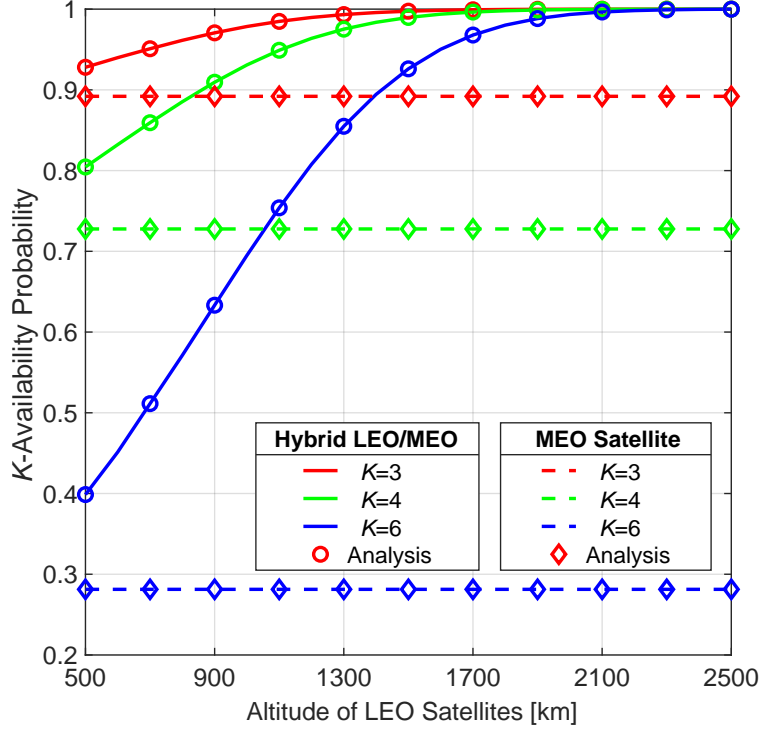


Fig. 4: K -availability probability for hybrid LEO/MEO satellite networks.

localizability performance. A constellation of more than 30 MEO satellites is already sufficient to ensure that both the 4-availability probability and the 4-localizability probability are close to 1. Additionally, an interesting finding is that changing the altitude of the MEO satellite constellation has little impact on localizability. The reason behind this phenomenon is that increasing the MEO constellation's altitude h_M , while enhancing availability, also weakens the received signal strength.

In Fig. 8, compared to a constellation with 12 MEO satellites at an altitude of $h_M = 20000$ km, the hybrid constellation with extra 2000 LEO satellites shows a gain in 3, 4, 6-localizability probability up to 10%, 27%, 60%, respectively. Due to the balance of availability and received signal strength, deploying the LEO satellite constellation at an altitude of about $h_L = 1500$ km can achieve the maximum gain in localizability performance.

Fig. 9 demonstrates the influence of numbers of LEO and MEO satellites on the 6-localizability probability, where $h_L = 2000$ km and $h_M = 20000$ km. In terms of localizability, the two types of satellites still show a complementary relationship in terms of quantity but do not exhibit a typical linear relationship as that in availability.

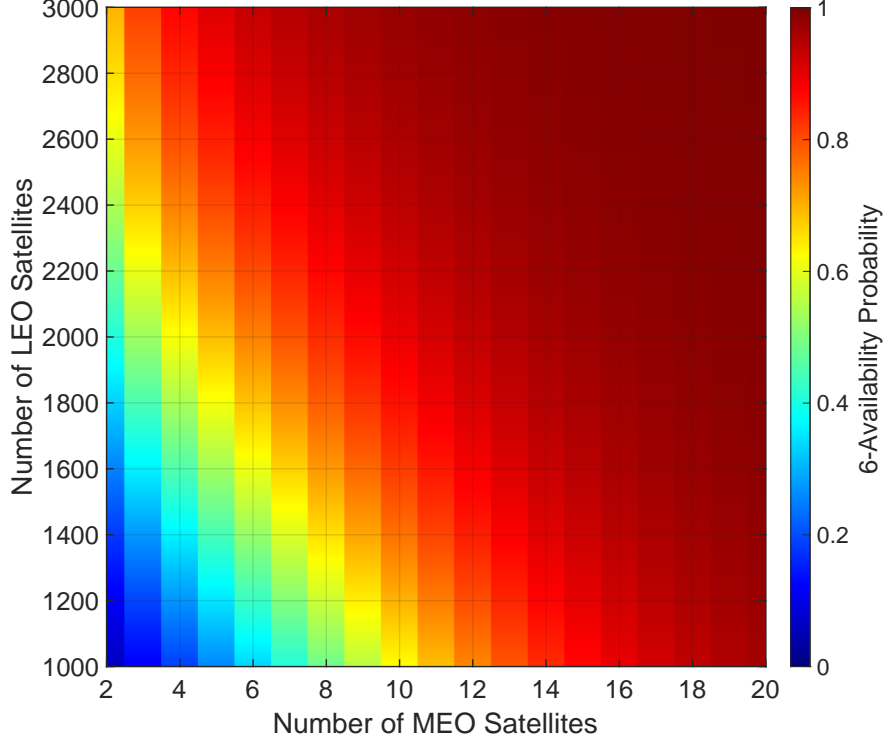


Fig. 5: Heatmap of 6-availability probability for hybrid LEO/MEO satellite networks.

V. FURTHER DISCUSSION

Building on the aforementioned statements, the primary contribution of this paper lies in proposing an analytical framework for studying satellite-enabled positioning issues and the DS-BPP model applicable to MEO satellite constellations. However, there are limitations in various aspects such as detailed modeling of channels and beams, design of positioning algorithms-based accuracy evaluation, and research on models based on SG. Therefore, we have dedicated this section further to delve deeper into these issues, which will also serve as a guide for future research.

A. Antenna Pattern

This subsection first presents four types of basic antenna patterns with their beam gain models in Table II, then designs a case study on the antenna patterns, followed by a discussion of the limitations of the beam-related analysis in this paper, serving as a direction for future improvements.

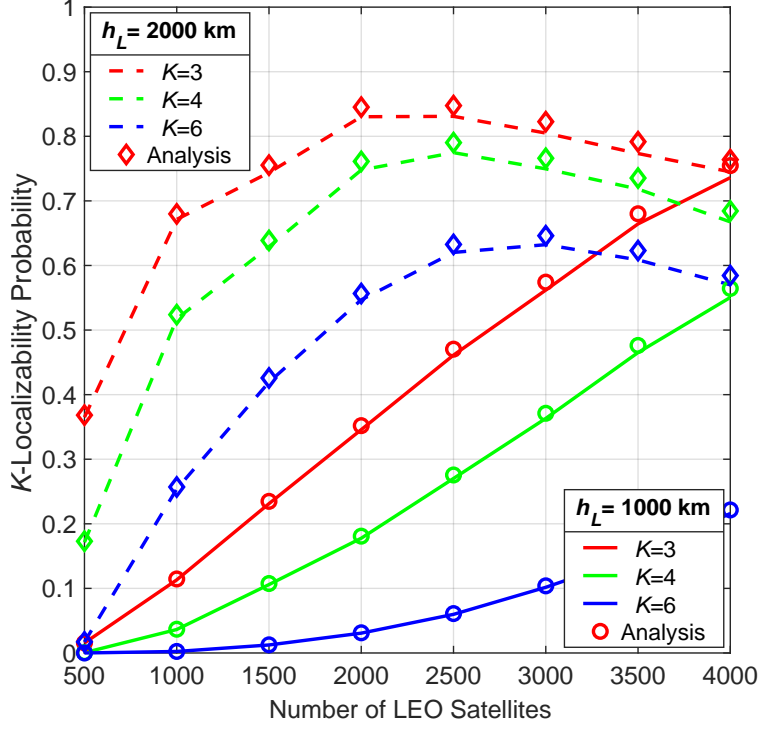


Fig. 6: K -localizability probability for LEO satellites.

TABLE II: Beam gains of basic antenna patterns.

Antenna Pattern	Model
Gaussian [32]	$G^r(\varphi^r) = G_L^m 2^{-(\varphi^r)^2 / \varphi_{3\text{dB}}^2}$
Flat-top [33]	$G^r(\varphi^r) = \begin{cases} G_L^m & \varphi^r \leq \varphi_{3\text{dB}} \\ 0 & \text{otherwise} \end{cases}$
Sinc [34]	$G^r(\varphi^r) = G_L^m \frac{\sin^2(\pi N_a \varphi^r)}{(\pi N_a \varphi^r)^2}$
Cosine [34]	$G(\varphi^r) = \begin{cases} G_L^m \cos^2\left(\frac{\pi N_a}{2} \varphi^r\right) & \varphi^r \leq \frac{1}{N_a} \\ 0 & \text{otherwise} \end{cases}$

In the numerical simulations of the previous section, the receiving beam gain was designed according to a Gaussian antenna pattern. Therefore, we extend this assumption to demonstrate that the analytical framework in this paper can be applied to various antenna patterns. As shown in Table II, N_a is defined as the number of antenna elements. Recall that G_L^m and $\varphi_{3\text{dB}}$ denote the maximum receiving antenna gain and the half-power beamwidth.

Next, we compare the impact of different antenna patterns on localizability probability in Fig. 10. To ensure consistency in the effective beamwidth, we set $N_a = 35$. φ_{max} follows the

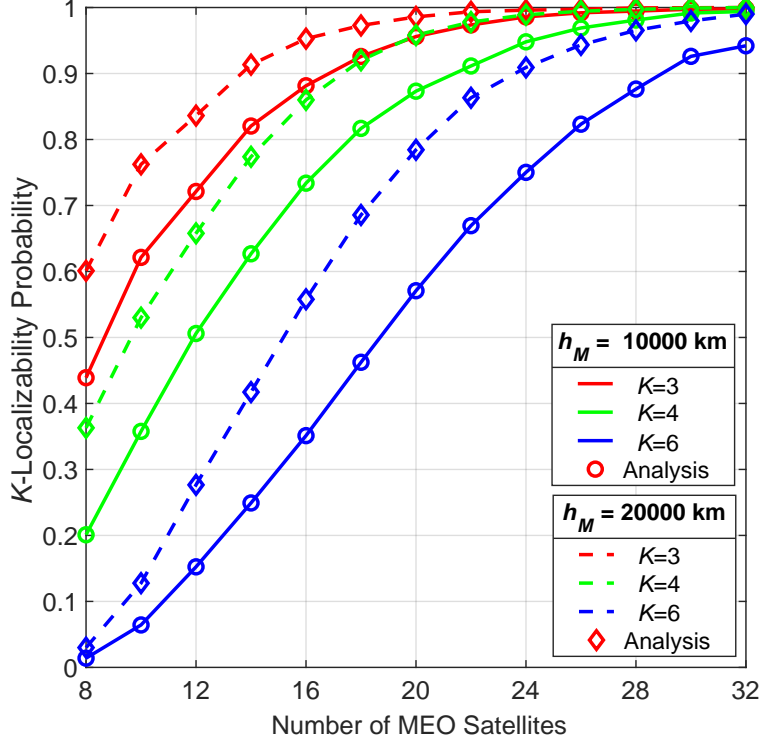


Fig. 7: K -localizability probability for MEO satellites.

default values in Table I, while N_a is set to 35. The effective receiving beam range φ_{\max} defined in (18) under different antenna patterns are given by

$$\varphi_{\max} = \begin{cases} 3\varphi_{3\text{dB}}, & \text{Gaussian,} \\ \varphi_{3\text{dB}}, & \text{Flat-top,} \\ \frac{3}{N_a}, & \text{Sinc,} \\ \frac{1}{N_a}, & \text{Cosine.} \end{cases} \quad (26)$$

Under the above parameter configuration, Fig. 10 shows the influences of antenna pattern and half-power beamwidth on 6-localizability probability. When the half-power beamwidth is larger, the beam is wider, and the interference signal from LEO satellites is stronger. Therefore, the 6-localizability probability decreases with the half-power beamwidth. Compared to half-power beamwidth, the effect of the antenna pattern on the localizability probability is much smaller. Moreover, the analytical results are greater than the simulated ones, and this phenomenon is also observed in Fig. 6 and Fig. 8. The main reason for this phenomenon is the approximation of interference. We only consider the impact of the closest interfering satellite on the localizability, while other interference sources are ignored. This leads to an underestimation of interference

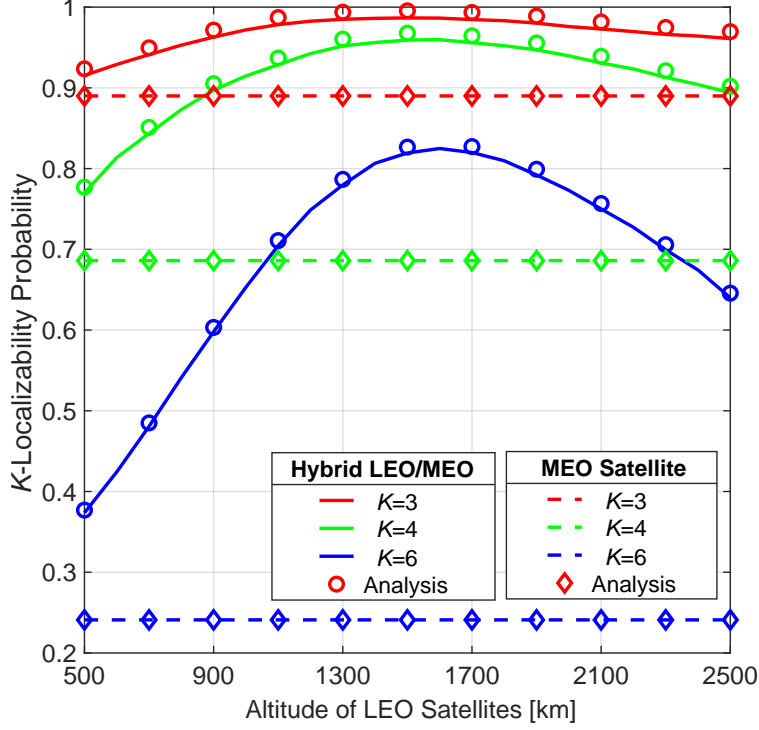


Fig. 8: K -localizability probability for hybrid LEO/MEO satellite networks.

and an overestimation of localizability availability. However, the deviation is only about 0.3%, which is within an acceptable range.

Finally, we point out the current limitations of beam gain modeling for further research and improvement. Firstly, the antenna patterns presented in Table II are relatively basic, and not common. The antenna patterns adopted in current LEO satellite constellations are carefully designed, dynamic, and adaptive. Additionally, these four antenna patterns are all circularly symmetric, whereas in most scenarios, they are functions of two angular variables, namely the azimuth angle and the elevation angle relative to the beam's steering direction [35]. Establishing a more meticulously designed beam gain model related to the satellite's latitude and longitude, along with developing an analytical framework based on it, represents a potential area for future research.

B. Positioning Error

The preceding analysis focuses on the unique challenges faced by stochastic geometry, the establishment of satellite spatial distribution and channel models, as well as the setup of satellite-enabled positioning problems. However, from the perspective of metrics, we are still focused

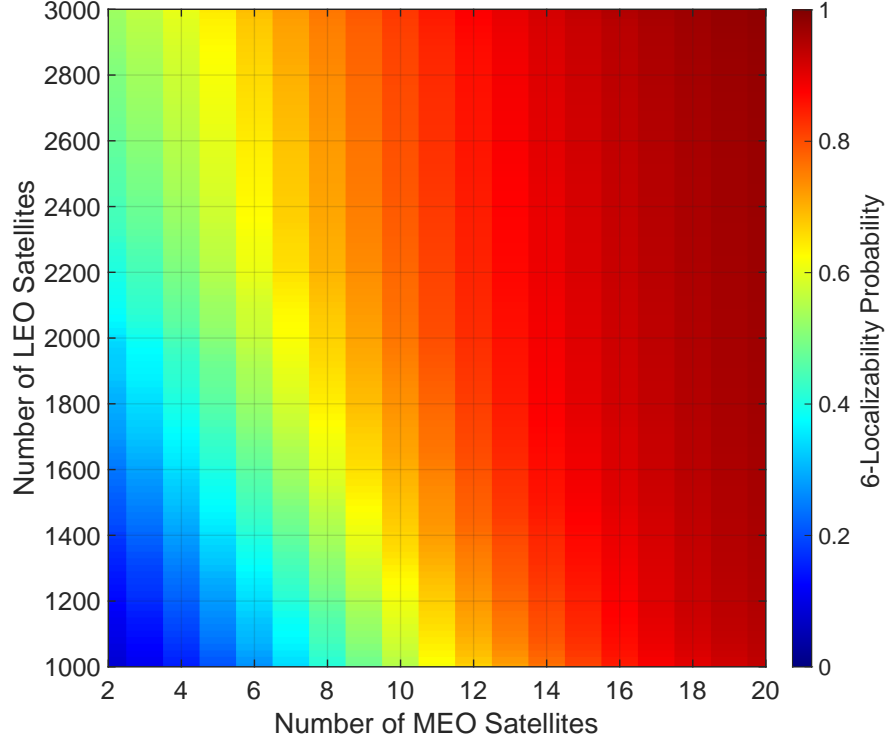


Fig. 9: Heatmap of 6-localizability probability for hybrid LEO/MEO satellite networks.

on fundamental positioning-related metrics such as availability and localizability, without delving into performance metrics related to positioning accuracy. Undoubtedly, in comparison to localizability, positioning accuracy receives more widespread attention and research interest. An increase in localizability probability implies that more satellites will participate in the positioning process, thereby enhancing positioning accuracy. However, establishing a direct mapping relationship between localizability probability and positioning accuracy is challenging, and similar conclusions have yet to be reached.

Fortunately, satellite-enabled positioning falls under geometric positioning, making positioning error suitable for analysis within the SG framework. Referring to research on terrestrial positioning systems based on stochastic geometry, two potential directions can be foreseen in the analysis of satellite-enabled positioning errors. The first direction involves the positioning error evaluation of specific geometric localization algorithms, such as the time difference of arrival algorithm. Along this research path, the core investigation may encompass estimating the probabilistic fuzzy region, also known as the circular error probable region [36].

The second direction involves researching topics related to positioning error analysis but is

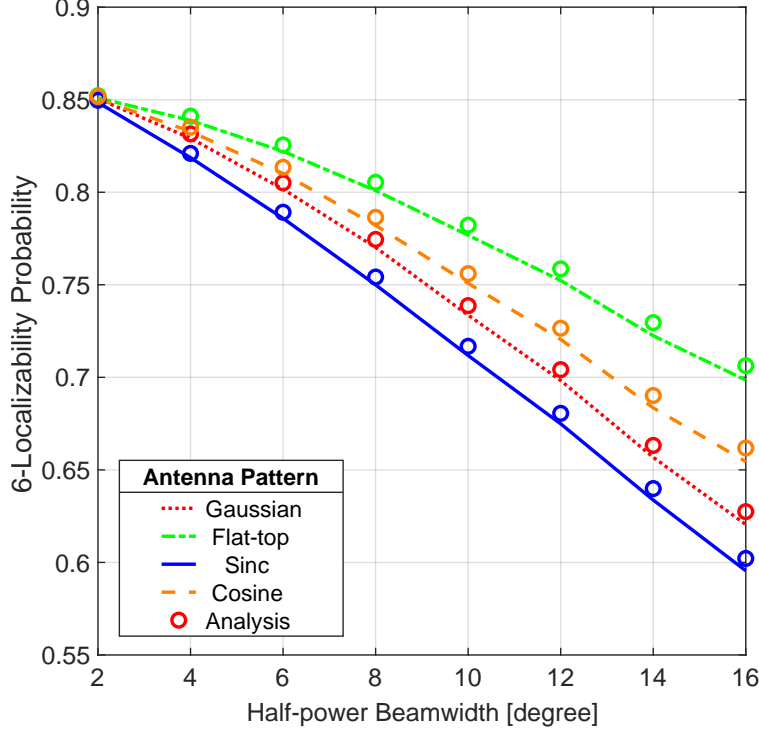


Fig. 10: Influence of antenna pattern on 6-localizability probability.

not confined to the performance metrics of specific positioning algorithms, aligning more closely with the principles of stochastic geometry. The variance of SINR and Cramér-Rao lower bound (CRLB) are two typical metrics that meet the above condition. The variance of SINR reflects the fluctuation of signal quality. A larger SINR variance typically indicates a higher fluctuation in signal quality, which can lead to increased positioning errors. The CRLB can be used to estimate the theoretical lower bound of errors for all positioning algorithms. So far, the latter has been utilized in the performance evaluation of ground positioning networks under a stochastic geometric framework [23].

Finally, we discuss the challenges of transitioning from localizability to positioning error analysis. Stochastic geometry typically characterizes channel randomness using statistical models. Therefore, statistical models like the SR fading model usually focus on describing the long-term impact of fading and shadowing effects on signal strength. Moreover, localizability probability is a long-term metric that considers random variations in satellite positions that typically occur over several hours. However, factors such as ionospheric scintillation can cause instantaneous fluctuations in signal phase and amplitude, leading to inaccuracies in signal arrival time measure-

ments by the receiver. Current statistical models have not yet accounted for this specific impact of ionospheric scintillation. Therefore, when dealing with critical factors affecting positioning accuracy like ionospheric scintillation, it is essential to not only consider its long-term effects through statistical models but also focus on its instantaneous impacts on positioning errors.

C. SG-Based Models

This section discusses recent advancements in point processes, a comparison between the CPP and DSBPP, and the implementation of DSBPP. In recent studies, point processes based on spherical stochastic geometry can be classified into non-orbital models [37], stochastic-orbital models [38], and fixed-orbital models [39]. The modeling accuracy of these three types of models increases gradually, but the complexity of deriving analytical expressions also correspondingly increases. When analyzing the time-correlated performance metrics of continuously moving satellites, the non-orbital model is no longer applicable. However, in scenarios involving complex topology analysis, such as routing, the strong tractability of the non-orbital model is essential. The stochastic-orbital model typically appears as a compromise choice, as in the context of this paper.

A detailed comparison of the strengths and weaknesses of DSBPP and CPP, both of which belong to stochastic orbital models, is also intriguing. CPP possesses many interesting mathematical characteristics, such as void probability and probability generating functional (PGFL), due to its Poisson randomness in quantity. These features play a crucial role in analyzing random variables like availability and interference, features that DSBPP lacks. Therefore, for a larger-scale LEO constellation like Starlink-1584, placed in 72 orbital planes with 22 satellites each, CPP is more tractable than DSBPP. Conversely, for a GPS MEO constellation composed of 6 orbital planes with 4 satellites each, assuming satellites on each orbital plane follow a Poisson distribution with a mean of 4 rather than being fixed at 4, would result in significant modeling differences. In such a scenario, DSBPP is preferred for modeling.

Finally, we present the implementation process of DSBPP in the form of MATLAB pseudo code. The following algorithm takes the number of orbits, the number of satellites on an orbit, and the distance between satellite and Earth center as inputs, and provides satellite positions as output.

Considering that the primary computational complexity of the algorithm stems from matrix multiplication, we define the complexity unit as one execution of step (12). As a result, the

Algorithm 1 DSBPP Generation Algorithm.

```

1: Input:  $N_o, N_M, R_M$ .
2: Initiate:  $Pos = \text{zeros}(3, N_o N_M)$ , and  $Index = 1$ .
3:  $Inc = \text{acos}(1 - 2 * \text{rand}(1, N_o)) / \pi * 180$ .
4:  $Azi = \text{rand}(N_o, 1) * 360$ .
5: for  $n = 1 : N_o$  do
6:    $Ang = \text{rand}(N_M, 1) * 360$ .
7:   for  $m = 1 : N_M$  do
8:      $x = R_M \cos(Ang(m))$ .
9:      $y = R_M \sin(Ang(m))$ .
10:     $z = 0$ .
11:     $Rx = [1, 0, 0; 0, \text{cosd}(Inc(n)), -\text{sind}(Inc(n)); 0, \text{sind}(Inc(n)), \text{cosd}(Inc(n))]$ .
12:     $Rz = [\text{cosd}(Azi(n)), -\text{sind}(Azi(n)), 0; \text{sind}(Azi(n)), \text{cosd}(Azi(n)), 0; 0, 0, 1]$ .
13:     $Loc = Rz * (Rx * [x; y; z])$ .
14:     $Pos(:, Index) = Loc$ .
15:     $Index = Index + 1$ .
16:   end for
17: end for
18: Output:  $Pos$ .

```

overall complexity of the algorithm is $\mathcal{O}(N_o N_M)$.

VI. CONCLUSION

In this paper, we developed an SG-based theoretical framework for the availability and localizability analysis of hybrid LEO/MEO satellite systems. We also validated the accuracy of our analysis via numerical simulations, which also demonstrate the availability and localizability performance of LEO, MEO, and hybrid LEO/MEO constellations. Additionally, the analysis allows us to create heatmaps to explore the impact of satellite numbers on the above metrics. Finally, we demonstrated the effects of the beam center angle and antenna pattern on network positioning. For future research directions, LEO satellites are expected to take on an increasing role in positioning services with the ongoing improvement of positioning technology. Furthermore, multiple LEO constellations may collaboratively participate in positioning. Therefore, it is

necessary to develop a more general association strategy for a hybrid constellation that includes multiple layers of LEO constellations and design a performance analysis framework based on this strategy within the SG framework.

APPENDIX A

PROOF OF LEMMA 1

In this proof, we study the upper limit of the central angle through the triangle formed by the Earth's center, satellite, and target. When the satellite is located at the horizon, this triangle forms a right-angled triangle, and $\theta_{Q,1}^{\max} = \arccos(R_{\oplus}/R_Q)$ in this case.

When the target is exactly located at the boundary of the satellite's main lobe beamwidth, the following equation can be obtained from the Law of Sines:

$$\frac{R_{\oplus}}{\sin(\frac{\varphi_Q}{2})} = \frac{R_Q}{\sin(\pi - \frac{\varphi_Q}{2} - \theta_{Q,2}^{\max})}. \quad (27)$$

When $0 < \pi - \frac{\varphi_Q}{2} - \theta_{Q,2}^{\max} < \pi$, there are two mappings from the sine value to the angle. When $\pi - \frac{\varphi_Q}{2} - \theta_{Q,2}^{\max} \leq \frac{\pi}{2}$ is an acute angle or a right angle, $\theta_{Q,2}^{\max} = \arccos(R_{\oplus}/R_Q)$. (ii) Otherwise, when $\pi - \frac{\varphi_Q}{2} - \theta_{Q,2}^{\max} > \frac{\pi}{2}$,

$$\begin{aligned} \theta_{Q,2}^{\max} &= \pi - \frac{\varphi_Q}{2} - \left(\pi - \arcsin\left(\frac{R_L \sin(\varphi_Q/2)}{R_{\oplus}}\right) \right) \\ &= \arcsin\left(\frac{R_L \sin(\varphi_Q/2)}{R_{\oplus}}\right) - \frac{\varphi_Q}{2}. \end{aligned} \quad (28)$$

It is not hard to prove that $\theta_{Q,2}^{\max} \leq \theta_{Q,1}^{\max}$ is always true.

APPENDIX B

PROOF OF LEMMA 2

To start with, we derive the probability of a single LEO satellite located in the spherical cap with a distance less than or equal to θ_L^{\max} from the ground target. From the definition of BPP [18],

$$\begin{aligned} \mathbb{P}[\theta \leq \theta_L^{\max}] &= \frac{\mathcal{A}(\mathcal{S}(\theta_L^{\max}))}{\mathcal{A}(\mathcal{S}(\pi))} \\ &= \frac{2\pi R_L^2 (1 - \cos \theta_L^{\max})}{4\pi R_L^2} = \frac{1 - \cos \theta_L^{\max}}{2}, \end{aligned} \quad (29)$$

where $\mathcal{S}(\theta)$ represents the spherical cap with a central angle of 2θ and $\mathcal{A}(\mathcal{S}(\theta))$ is the area measure of $\mathcal{S}(\theta)$. Considering that each LEO satellite located within the spherical cap $\mathcal{S}(\theta_L^{\max})$

is an independent event, the K -availability probability of LEO satellite networks can be obtained through the CDF of the binomial distribution:

$$\begin{aligned}
 P_L^A(K) &= 1 - \sum_{k=0}^{K-1} \mathbb{P}[\mathcal{N}(\mathcal{S}(\theta_L^{\max})) = k] \\
 &= 1 - \sum_{k=0}^{K-1} \binom{N_L}{k} \left(\frac{1 - \cos \theta_L^{\max}}{2} \right)^k \\
 &\quad \times \left(1 - \frac{1 - \cos \theta_L^{\max}}{2} \right)^{N_L - k},
 \end{aligned} \tag{30}$$

where $\mathcal{N}(\mathcal{S}(\theta_L^{\max}))$ counts the number of LEO satellites in the sperical cap $\mathcal{S}(\theta_L^{\max})$.

APPENDIX C

PROOF OF LEMMA 3

The proof of Lemma 3 is divided into two steps: (i) Derive the critical condition for the existence of available satellites; (ii) Derive the maximum central angle $\theta_{c,M}^{\max}(\theta_{\perp}, d_M^{\max})$.

If the normal vector of the orbit is perpendicular to the typical target ($\theta_{\perp} = \frac{\pi}{2}$), the satellite moving trajectory will pass the overhead of the target. In this case, the typical target has the maximum satellite availability probability. As θ_{\perp} decreases, the orbit will progressively deviate from the target's overhead. To ensure there exist available satellites for the target,

$$\left| \theta_{\perp} - \frac{\pi}{2} \right| \leq \theta_{\perp, \min} \tag{31}$$

needs to be satisfied. When $\theta_{\perp} = \theta_{\perp, \min}$, the closest position on the orbit has a distance d_{\max} to the target. As shown at the left part of Fig. 11, we can present $\theta_{\perp, \min}$ by the law of cosines,

$$\frac{\pi}{2} - \theta_{\perp, \min} = \arccos \left(\frac{R_s^2 + R_{\oplus}^2 - (d_M^{\max})^2}{2R_s R_{\oplus}} \right). \tag{32}$$

Therefore, the critical condition for the existence of available satellites is

$$\left| \theta_{\perp} - \frac{\pi}{2} \right| \leq \arcsin \left(\frac{R_s^2 + R_{\oplus}^2 - (d_M^{\max})^2}{2R_s R_{\oplus}} \right). \tag{33}$$

Next, we derive the analytical expression for the maximum central angle. As shown in the right part of Fig. 11, we denote the center of the Earth as O and the position of the target as D . A and B are the critical positions in the orbit where satellites can maintain communication with the target. From the definition, we have $\overline{AD} = \overline{BD} = d_M^{\max}$, where \overline{AD} is the length of the line segment AD . We draw a perpendicular from the midpoint C of line segment AB to the

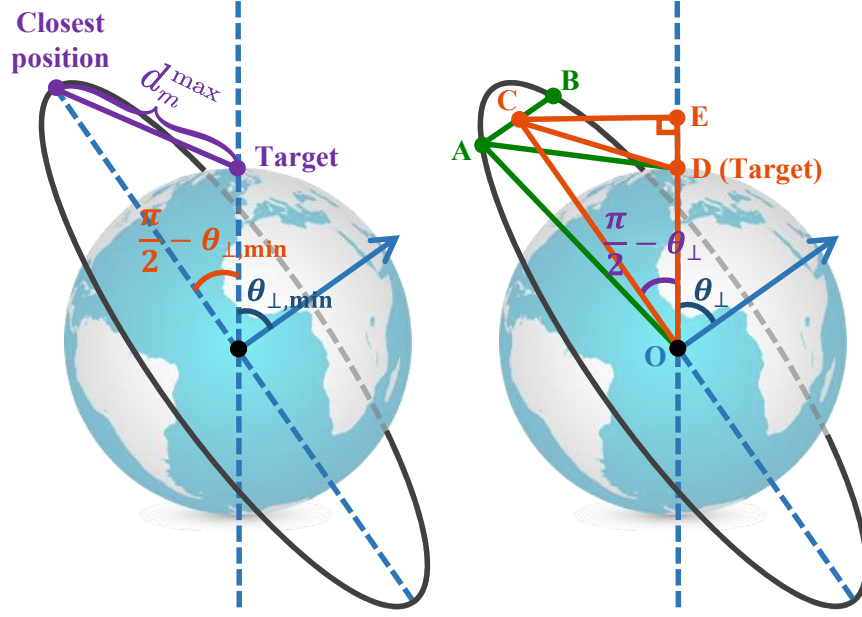


Fig. 11: Illustration of the critical condition and maximum central angle.

line OD , and the point of intersection is denoted as E . By the geometric relationship in right triangles $\triangle COE$ and $\triangle CDE$, it can be known that:

$$\begin{cases} \overline{CE} = \overline{OC} \cos \theta_{\perp}, \\ \overline{OE} = \overline{OC} \sin \theta_{\perp} = \overline{DE} + R_{\oplus}, \\ \overline{DC}^2 = \overline{DE}^2 + \overline{CE}^2. \end{cases} \quad (34)$$

Thus, we get

$$\overline{DC}^2 = \overline{OC}^2 + R_{\oplus}^2 - 2\overline{OC} \sin \theta_{\perp} R_{\oplus}. \quad (35)$$

By the geometric relationship in right triangles $\triangle AOC$ and $\triangle ADC$, it can be known that:

$$\overline{DC}^2 = \overline{AD}^2 + \overline{OC}^2 - \overline{AO}^2 = d_{\max}^2 + \overline{OC}^2 - R_s^2. \quad (36)$$

By combining (35) and (36), we get

$$\overline{OC} = \frac{R_{\oplus}^2 + R_s^2 - (d_{\max}^{\max})^2}{2R_{\oplus} \sin \theta_{\perp}}. \quad (37)$$

Then, the maximum central angle for two available satellites in the orbit can be derived,

$$\theta_{c,M}^{\max}(\theta_{\perp}, d_M^{\max}) = 2 \arccos \left(\frac{\overline{OC}}{\overline{OA}} \right) = 2 \arccos \left(\frac{R_{\oplus}^2 + R_s^2 - d_{\max}^2}{2R_{\oplus} R_s \sin \theta_{\perp}} \right). \quad (38)$$

Please note that the above letters ($O, A \sim F$) and symbols (such as \overline{AB}) are only defined for the convenience of theorem proof. Their meanings are different from those of letters and symbols in other parts of the article.

APPENDIX D

PROOF OF LEMMA 4

In this proof, we derive the probability that the distance from a single MEO satellite to the target is less than θ_M^{\max} . Given that an MEO satellite is located on an orbit with inclination angle θ_{\perp} , the probability that this MEO satellite is available to the target is $\theta_{c,M}^{\max}(\theta_{\perp}, d_M^{\max})/(2\pi)$. Therefore, the probability that a single MEO satellite is available for the target is

$$p_{M,1}^A = \mathbb{E}_{\theta_{\perp}} \left[\frac{\theta_{c,M}^{\max}(\theta_{\perp}, d_M^{\max})}{2\pi} \right] = \int_{\frac{\pi}{2} - \arccos\left(\frac{R_{\oplus}^2 + R_M^2 - (d_M^{\max})^2}{2R_{\oplus}R_M}\right)}^{\frac{\pi}{2} + \arccos\left(\frac{R_{\oplus}^2 + R_M^2 - (d_M^{\max})^2}{2R_{\oplus}R_M}\right)} \frac{\sin \theta}{2} \frac{\theta_{c,M}^{\max}(\theta, d_M^{\max})}{2\pi} d\theta. \quad (39)$$

Note that the upper and lower bounds of integral in (39) come from the fact that $\theta_{c,M}^{\max}(\theta_{\perp}, d_M^{\max}) \neq 0$ when

$$\left| \theta_{\perp} - \frac{\pi}{2} \right| \leq \arccos \left(\frac{R_{\oplus}^2 + R_M^2 - (d_M^{\max})^2}{2R_{\oplus}R_M} \right). \quad (40)$$

Similarly, the probability of exactly k available MEO satellites $p_M^A(k)$ can also be obtained using the CDF of the binomial distribution:

$$P_M^A(K) = 1 - \sum_{k=0}^{K-1} \binom{N_M N_O}{k} (p_{M,1}^A)^k (1 - p_{M,1}^A)^{N_M N_O - k}. \quad (41)$$

APPENDIX E

PROOF OF THEOREM 1

The K -availability probability for the hybrid LEO/MEO satellite networks can be categorized into the following two conditions:

- When the number of available MEO satellites is greater than K , the K -availability is met regardless of the availability of LEO satellites. This condition happens with probability

$$P_{\text{all},1}^A(K) = \sum_{k=K}^{\min\{K, N_M^{\max}\}} p_M^A(k), \quad (42)$$

where $p_M^A(k)$ can be obtained by probability mass function (PMF) of the binomial distribution,

$$p_M^A(k) = \binom{N_M N_O}{k} (p_{M,1}^A)^k (1 - p_{M,1}^A)^{N_M N_O - k}. \quad (43)$$

$$\begin{aligned}
f_{\theta_L}^{(k)}(\theta) &= 1 - \frac{1}{2^{N_L}} \sum_{n=0}^{k-1} \binom{N_L}{n} \times \left((1 - \cos \theta)^n \frac{d(1 + \cos \theta)^{N_L-n}}{d\theta} + (1 + \cos \theta)^{N_L-n} \frac{d(1 - \cos \theta)^n}{d\theta} \right) \\
&= 1 - \frac{\sin \theta}{2^{N_L}} \sum_{n=0}^{k-1} \binom{N_L}{n} \left(n(1 + \cos \theta)^{N_L-n} (1 - \cos \theta)^{n-1} - (N_L - n)(1 - \cos \theta)^n (1 + \cos \theta)^{N_L-n-1} \right) \quad (47) \\
&= 1 - \frac{\sin \theta}{2^{N_L}} \sum_{n=0}^{k-1} \binom{N_L}{n} (1 - \cos \theta)^n (1 + \cos \theta)^{N_L-n} \left(\frac{n}{1 - \cos \theta} - \frac{N_L - n}{1 + \cos \theta} \right).
\end{aligned}$$

- If exactly $k < K$ MEO satellites are available, the probability of achieving k -availability in a hybrid constellation is equivalent to the probability of having at least $K - k$ available LEO satellites. By traversing the available quantities of MEO satellites k , this condition happens with probability

$$P_{\text{all},2}^A(K) = \sum_{k=0}^{\min\{K-1, N_M^{\max}-1\}} P_L^A(K-k) p_M^A(k). \quad (44)$$

The final K -availability probability of the hybrid constellation can be obtained by

$$P_{\text{all}}^A(K) = P_{\text{all},1}^A(K) + P_{\text{all},2}^A(K). \quad (45)$$

APPENDIX F

PROOF OF LEMMA 5

According to the CDF of the binomial distribution, the CDF of k -LEO contact angle distribution is derived as,

$$\begin{aligned}
F_{\theta_L}^{(k)}(\theta) &= 1 - \sum_{n=0}^{k-1} \mathbb{P}[\mathcal{N}(\mathcal{S}(\theta)) = n] \\
&= 1 - \sum_{n=0}^{k-1} \binom{N_L}{n} \left(\frac{1 - \cos \theta}{2} \right)^n \left(\frac{1 + \cos \theta}{2} \right)^{N_L-n}. \quad (46)
\end{aligned}$$

where $\mathcal{S}(\theta)$ denotes the spherical cap with a central angle of 2θ , and $\mathcal{N}(\mathcal{S}(\theta))$ counts the number of LEO satellites $\mathcal{S}(\theta)$. Take the derivative of $F_{\theta_L}^{(k)}(\theta)$ yields the PDF of the contact angle distribution, which is given in (47) at the top of the next page.

APPENDIX G
PROOF OF LEMMA 6

To start with, we derive the conditional MEO contact angle distribution for a given inclination angle,

$$\begin{aligned}
 F_{\theta_M}(\theta | \theta_\perp) &= \mathbb{P}[\theta_M \leq \theta | \theta_\perp] \\
 &= \frac{1}{2\pi} \theta_{c,M}^{\max} \left(\theta_\perp, \sqrt{R_M^2 + R_\oplus^2 - 2R_MR_\oplus \cos \theta} \right) \\
 &= \frac{1}{\pi} \arccos \left(\frac{\cos \theta}{\sin \theta_\perp} \right), \quad \theta \leq \theta_M^{\max},
 \end{aligned} \tag{48}$$

where $\theta_{c,M}^{\max}(\theta_\perp, l(\theta))$ is derived in Lemma 3, and $l(\theta) = \sqrt{R_M^2 + R_\oplus^2 - 2R_MR_\oplus \cos \theta}$ denotes the Euclidean distance between the MEO satellite and target given that the central angle between them is θ .

On an orbit with an inclination angle of θ_\perp , the minimum contact angle from an MEO satellite to the target is $|\frac{\pi}{2} - \theta_\perp|$. If there exist an MEO satellite with MEO contact angle $\theta_M \leq \theta$, the range of inclination angle should satisfy $|\frac{\pi}{2} - \theta_\perp| \leq \theta$. Therefore, the unconditional MEO contact angle distribution can be obtained by

$$\begin{aligned}
 F_{\theta_M}(\theta) &= \int_{\frac{\pi}{2}-\theta}^{\frac{\pi}{2}+\theta} \frac{\sin \theta_\perp}{2} \frac{1}{\pi} \arccos \left(\frac{\cos \theta}{\sin \theta_\perp} \right) d\theta_\perp \\
 &= \int_{\frac{\pi}{2}-\theta}^{\frac{\pi}{2}} \frac{\sin \theta_\perp}{\pi} \arccos \left(\frac{\cos \theta}{\sin \theta_\perp} \right) d\theta_\perp.
 \end{aligned} \tag{49}$$

According to the Leibniz integral rule, the PDF of MEO contact angle distribution can be obtained by taking the derivative of the CDF,

$$\begin{aligned}
 f_{\theta_M}(\theta) &= \int_{\frac{\pi}{2}-\theta}^{\frac{\pi}{2}} \frac{\sin \theta_\perp}{\pi} \frac{d}{d\theta} \left(\arccos \left(\frac{\cos \theta}{\sin \theta_\perp} \right) \right) d\theta_\perp \\
 &\quad - \frac{d \left(\frac{\pi}{2} - \theta \right)}{d\theta} \times \frac{\sin \left(\frac{\pi}{2} - \theta \right)}{\pi} \arccos \left(\frac{\cos \theta}{\sin \left(\frac{\pi}{2} - \theta \right)} \right) \\
 &\stackrel{(a)}{=} \frac{1}{\pi} \int_{\frac{\pi}{2}-\theta}^{\frac{\pi}{2}} \sin \theta_\perp \frac{d}{d\theta} \left(\arccos \left(\frac{\cos \theta}{\sin \theta_\perp} \right) \right) d\theta_\perp \\
 &= \frac{1}{\pi} \int_{\frac{\pi}{2}-\theta}^{\frac{\pi}{2}} \sin \theta_\perp \frac{\sin \theta}{\sqrt{1 - \left(\frac{\cos \theta}{\sin \theta_\perp} \right)^2}} d\theta_\perp,
 \end{aligned} \tag{50}$$

where step (a) comes from

$$\arccos \left(\frac{\cos \theta}{\sin \left(\frac{\pi}{2} - \theta \right)} \right) = \arccos \left(\frac{\cos \theta}{\cos \theta} \right) = 0. \tag{51}$$

APPENDIX H

PROOF OF LEMMA 7

The proof is divided into the following steps:

- Introduce the concept of effective receiving beam range.
- Establish the relationship between the dome angle and the central angle.
- Analyze the two most likely conditions and their probabilities for the distribution of interfering satellites.
- Derive the PDF of the interference power distribution.

Note that The dome angle between A and B is the angle created by the line connecting A to the ground target and the line connecting B to the ground target. Taking the Gaussian antenna pattern as an example, When $\varphi^r > 3\varphi_{3\text{dB}}$, $G^r(\varphi^r) < 2^{-9} G_L^m$. Therefore, power from interfering satellites with dome angle beyond $\varphi_{\max} = 3\varphi_{3\text{dB}}$ at the target can be neglected due to the excessively low receiving antenna gain. For other patterns in Table II, we consider $\varphi_{\max} = \varphi_{3\text{dB}}$ for Flat-top antenna, $\varphi_{\max} = \frac{3}{N_a}$ for Sinc antenna (including main lobe and the first side lobe), and $\varphi_{\max} = \frac{1}{N_a}$ for Cosine antenna.

Then, relationship between central angle θ_d^{\max} and the corresponding dome angle φ_{\max} can be given through the sine rule [40],

$$\varphi_{\max} = \cot^{-1} \left(\cot \theta_d^{\max} - \frac{R_{\oplus}}{R_L} \sqrt{1 + \cot^2 \theta_d^{\max}} \right). \quad (52)$$

By applying the inverse operation, the result is as follows:

$$\begin{aligned} \theta_d^{\max} = \cot^{-1} & \left(\frac{R_L^2}{R_L^2 - R_{\oplus}^2} \left(\cot \varphi_{\max} \right. \right. \\ & \left. \left. + \sqrt{(R_{\oplus}/R_L)^2 (1 + \cot^2 \varphi_{\max} - (R_{\oplus}/R_L)^2)} \right) \right). \end{aligned} \quad (53)$$

To reduce computational complexity, we consider the two most likely conditions to approximate the interference power distribution: there is zero or one available LEO satellite within the effective receiving beam range. Typically, the number of satellites in MEO constellations is much smaller than that in LEO constellations. Therefore, under the narrow beam assumption, we omit the availability of MEO satellites. Similar to the proof of Lemma 2, the probability of having no satellites in the effective receiving beam range is

$$\begin{aligned} P_{\varphi}^{(0)}(\theta_d^{\max}) &= \mathbb{P} [\mathcal{N}(\mathcal{S}(\theta_d^{\max})) = 0] \\ &= \left(1 - \frac{2\pi R_L^2 (1 - \cos \theta_d^{\max})}{4\pi R_L^2} \right)^{N_L} = \left(\frac{1 + \cos \theta_d^{\max}}{2} \right)^{N_L}. \end{aligned} \quad (54)$$

The above deduction is based on the spherical cap approximation of the beam shape under the narrow-beam assumption. The probability of having one satellite can be approximately considered as $P_\varphi^{(1)} \approx 1 - P_\varphi^{(0)}$.

Finally, when the central angle of the effective receiving beam range is θ_d^{\max} , the interference power $I(\theta_d^{\max}) = 0$ with probability $P_\varphi^{(0)}(\theta_d^{\max})$. Given that there is one satellite within the effective receiving beam range, the CDF of the central angle between the associated satellite and the interfering satellite is

$$F_{\theta_I}(\theta) = \frac{2\pi R_L^2(1 - \cos \theta)}{2\pi R_L^2(1 - \cos \theta_d^{\max})} = \frac{1 - \cos \theta}{1 - \cos \theta_d^{\max}}, \quad (55)$$

where $0 \leq \theta \leq \theta_d^{\max}$. Given that the central angle between the associated satellite and the interfering satellite is θ_I , the interference power can be approximately expressed as

$$I_{\theta_I} = \frac{\rho_L^t G_L^t \zeta \left(\frac{\lambda_L}{4\pi}\right)^2 W}{R_L^2 + R_\oplus^2 - 2R_L R_\oplus \cos \theta_L} \times G^r \left(\cot^{-1} \left(\cot \theta_I - \frac{R_\oplus}{R_L} \sqrt{1 + \cot^2 \theta_I} \right) \right), \quad (56)$$

where θ_L is the central angle between the associated satellite and the target. Therefore, the CDF of the interference power distribution is

$$\begin{aligned} F_I(I) &= \mathbb{E}_{\theta_I} [I_{\theta_I} < I] \\ &= \int_0^{\theta_d^{\max}} \frac{\sin \theta_I}{1 - \cos \theta_d^{\max}} F_W \left(I \frac{R_L^2 + R_\oplus^2 - 2R_L R_\oplus \cos \theta_L}{\rho_L^t G_L^t \zeta \left(\frac{\lambda_L}{4\pi}\right)^2} \right. \\ &\quad \left. \times \left(G^r \left(\cot^{-1} \left(\cot \theta_I - \frac{R_\oplus}{R_L} \sqrt{1 + \cot^2 \theta_I} \right) \right) \right)^{-1} \right) d\theta_I. \end{aligned} \quad (57)$$

The PDF of interference power distribution can be obtained by taking the derivative of (57) with respect to I .

APPENDIX I

PROOF OF LEMMA 8

First, we start the derivation from the localizability probability for the k -nearest satellites to the target:

$$\begin{aligned}
 p_L^C(k) &= \mathbb{E}_{I, \theta_L} \left[\mathbb{P} \left[\left(\frac{\lambda_L}{4\pi} \right)^2 \frac{1}{(I + \sigma_L^2)} \right. \right. \\
 &\quad \times \left. \left. \frac{\rho_L^t G_L^t G_L^m \zeta W}{(R_L^2 + R_\oplus^2 - 2R_L R_\oplus \cos \theta_L)} > \gamma_L \right] \right] \\
 &= \int_0^{\theta_L^{\max}} f_{\theta_L}^{(k)}(\theta) \int_0^\infty f_I(I) \left(1 - F_W \left(\gamma_L \left(\frac{4\pi}{\lambda_L} \right)^2 \right. \right. \\
 &\quad \times \left. \left. \frac{(I + \sigma_L^2)(R_L^2 + R_\oplus^2 - 2R_L R_\oplus \cos \theta_L)}{\rho_L^t G_L^t G_L^m \zeta} \right) \right) dI d\theta_L.
 \end{aligned} \tag{58}$$

From the definition, the K -localizability probability for the LEO satellite constellation is

$$P_L^C(K) = \prod_{k=1}^K p_L^C(k). \tag{59}$$

REFERENCES

- [1] C. Cai, Y. Gao, L. Pan, and J. Zhu, “Precise point positioning with quad-constellations: GPS, BeiDou, GLONASS and Galileo,” *Advances in space research*, vol. 56, no. 1, pp. 133–143, 2015.
- [2] R. M. Ferre, E. S. Lohan, H. Kuusniemi, J. Praks, S. Kaasalainen, C. Pinell, and M. Elsanhoury, “Is LEO-based positioning with mega-constellations the answer for future equal access localization?” *IEEE Communications Magazine*, vol. 60, no. 6, pp. 40–46, 2022.
- [3] Y. Liao, S. Liu, X. Hong, J. Shi, and L. Cheng, “Integration of communication and navigation technologies toward LEO-enabled 6G networks: A survey,” *Space: Science & Technology*, vol. 3, p. 0092, 2023.
- [4] F. Yue, Z. Cui, S. Li, H. Jing, S. Zhang, and M. Wang, “A satellite augmentation system based on LEO mega-constellation,” in *Proc. IEEE International Conference on Artificial Intelligence, Information Processing and Cloud Computing (AIIPCC)*, 2022, pp. 221–225.
- [5] T. G. Reid, A. M. Neish, T. Walter, and P. K. Enge, “Broadband LEO constellations for navigation,” *NAVIGATION: Journal of the Institute of Navigation*, vol. 65, no. 2, pp. 205–220, 2018.
- [6] R. M. Ferre and E. S. Lohan, “Comparison of MEO, LEO, and terrestrial IoT configurations in terms of gdop and achievable positioning accuracies,” *IEEE Journal of Radio Frequency Identification*, vol. 5, no. 3, pp. 287–299, 2021.
- [7] C. Specht, M. Mania, M. Skóra, and M. Specht, “Accuracy of the gps positioning system in the context of increasing the number of satellites in the constellation,” *Polish Maritime Research*, vol. 22, no. 2, pp. 9–14, 2015.
- [8] N. Raghu, B. Kiran, and K. Manjunatha, “Tracking of IRNSS, GPS and hybrid satellites by using IRNSS receiver in STK simulation,” in *International Conference on Communication and Signal Processing (ICCSP)*. IEEE, 2016, pp. 0891–0896.
- [9] H. Halevi, I. Bergel, and Y. Noam, “Asymptotic performance of TDOA estimation using satellites,” *IEEE Transactions on Signal Processing*, vol. 70, pp. 2349–2361, 2022.

- [10] Q. Wei, X. Chen, C. Jiang, and Z. Huang, "Time-of-arrival estimation for integrated satellite navigation and communication signals," *IEEE Transactions on Wireless Communications*, 2023.
- [11] V. R. Chandrika, J. Chen, L. Lampe, G. Vos, and S. Dost, "SPIN: Synchronization signal based positioning algorithm for IoT non-terrestrial networks," *IEEE Internet of Things Journal*, 2023.
- [12] B. Al Homssi, A. Al-Hourani, K. Wang, P. Conder, S. Kandeepan, J. Choi, B. Allen, and B. Moores, "Next generation mega satellite networks for access equality: Opportunities, challenges, and performance," *IEEE Communications Magazine*, vol. 60, no. 4, pp. 18–24, 2022.
- [13] R. Wang, M. A. Kishk, and M.-S. Alouini, "Ultra-dense LEO satellite-based communication systems: A novel modeling technique," *IEEE Communications Magazine*, vol. 60, no. 4, pp. 25–31, 2022.
- [14] A. Al-Hourani, "Optimal satellite constellation altitude for maximal coverage," *IEEE Wireless Communications Letters*, vol. 10, no. 7, pp. 1444–1448, 2021.
- [15] R. Wang, M. A. Kishk, and M.-S. Alouini, "Modeling and analysis of non-terrestrial networks by spherical stochastic geometry," 2025, available online: <https://arxiv.org/abs/2503.13455>.
- [16] A. Talgat, M. A. Kishk, and M.-S. Alouini, "Stochastic geometry-based analysis of LEO satellite communication systems," *IEEE Communications Letters*, vol. 25, no. 8, pp. 2458–2462, 2021.
- [17] R. Wang, M. A. Kishk, and M.-S. Alouini, "Evaluating the accuracy of stochastic geometry based models for LEO satellite networks analysis," *IEEE Communications Letters*, vol. 26, no. 10, pp. 2440–2444, 2022.
- [18] N. Okati, T. Riihonen, D. Korpi, I. Angervuori, and R. Wichman, "Downlink coverage and rate analysis of low Earth orbit satellite constellations using stochastic geometry," *IEEE Transactions on Communications*, vol. 68, no. 8, pp. 5120–5134, 2020.
- [19] C.-S. Choi and F. Baccelli, "A novel analytical model for leo and meo satellite networks based on cox point processes," *IEEE Transactions on Communications*, 2024, early Access.
- [20] C.-S. Choi, "Modeling and analysis of downlink communications in a heterogeneous LEO satellite network," *IEEE Transactions on Wireless Communications*, 2024, early access.
- [21] D.-H. Jung, H. Nam, J. Choi, and D. J. Love, "Modeling and analysis of GEO satellite networks," available online: <https://arxiv.org/abs/2312.15924>.
- [22] J. Schloemann, H. S. Dhillon, and R. M. Buehrer, "Localization performance in cellular networks," in *Proc. IEEE International Conference on Communication Workshop (ICCW)*, 2015, pp. 871–876.
- [23] E. Christopher, H. S. Dhillon, and R. M. Buehrer, "A statistical characterization of localization performance in wireless networks," *IEEE Transactions on Wireless Communications*, vol. 17, no. 9, pp. 5841–5856, 2018.
- [24] J. Schloemann, H. S. Dhillon, and R. M. Buehrer, "Toward a tractable analysis of localization fundamentals in cellular networks," *IEEE Transactions on Wireless Communications*, vol. 15, no. 3, pp. 1768–1782, 2015.
- [25] A. Talgat, M. A. Kishk, and M.-S. Alouini, "Nearest neighbor and contact distance distribution for binomial point process on spherical surfaces," *IEEE Communications Letters*, vol. 24, no. 12, pp. 2659–2663, 2020.
- [26] N. Okati and T. Riihonen, "Nonhomogeneous stochastic geometry analysis of massive LEO communication constellations," *IEEE Transactions on Communications*, vol. 70, no. 3, pp. 1848–1860, 2022.
- [27] R. Wang, M. A. Kishk, and M.-S. Alouini, "Stochastic geometry-based low latency routing in massive LEO satellite networks," *IEEE Transactions on Aerospace and Electronic Systems*, vol. 58, no. 5, pp. 3881–3894, 2022.
- [28] W. Feller, *An introduction to probability theory and its applications, Volume 2*. John Wiley & Sons, 1991, vol. 81.
- [29] A. Abdi, W. C. Lau, M.-S. Alouini, and M. Kaveh, "A new simple model for land mobile satellite channels: First-and second-order statistics," *IEEE Transactions on Wireless Communications*, vol. 2, no. 3, pp. 519–528, 2003.

- [30] A. Almagbile, J. Wang, and W. Ding, "Evaluating the performances of adaptive Kalman filter methods in GPS/INS integration," *Journal of Global Positioning Systems*, vol. 9, no. 1, pp. 33–40, 2010.
- [31] S. Singhal, S. K. Biswas, and S. S. Ram, "LEO/MEO-based multi-static passive radar detection performance analysis using stochastic geometry," in *Radar Conference (RadarConf23)*. IEEE, 2023, pp. 1–6.
- [32] R. M. Gagliardi, *Satellite communications*. Springer Science & Business Media, 2012.
- [33] C. A. Balanis, *Antenna theory: analysis and design*. John wiley & sons, 2015.
- [34] X. Yu, J. Zhang, M. Haenggi, and K. B. Letaief, "Coverage analysis for millimeter wave networks: The impact of directional antenna arrays," *IEEE Journal on Selected Areas in Communications*, vol. 35, no. 7, pp. 1498–1512, 2017.
- [35] E. Kim, I. P. Roberts, and J. G. Andrews, "Downlink analysis and evaluation of multi-beam LEO satellite communication in shadowed Rician channels," *IEEE Transactions on Vehicular Technology*, vol. 73, no. 2, pp. 2061–2075, 2024.
- [36] J. S. Lewis, J. L. Rachlow, E. O. Garton, and L. A. Vierling, "Effects of habitat on GPS collar performance: using data screening to reduce location error," *Journal of applied ecology*, vol. 44, no. 3, pp. 663–671, 2007.
- [37] J. Yim, J. Park, and N. Lee, "Modeling and coverage analysis of K-tier integrated satellite-terrestrial downlink networks," 2024, available online: <https://arxiv.org/abs/2403.11096>.
- [38] C.-S. Choi, "Analysis of a delay-tolerant data harvest architecture leveraging low earth orbit satellite networks," *IEEE Journal on Selected Areas in Communications*, vol. 42, no. 5, pp. 1329–1343, 2024.
- [39] Y. Sun and R. Li, "Performance analysis of satellite-terrestrial integrated radio access networks based on stochastic geometry," 2024, available online: <https://arxiv.org/abs/2404.09506>.
- [40] A. Al-Hourani, "An analytic approach for modeling the coverage performance of dense satellite networks," *IEEE Wireless Communications Letters*, vol. 10, no. 4, pp. 897–901, 2021.